Chapter

The Tungsten-Based Plasma-Facing Materials

Tao Zhang, Zhuoming Xie, Changsong Liu and Ying Xiong

Abstract

The plasma-facing materials in fusion reactors will face very extreme servicing condition such as high temperatures, high thermal loads, extreme irradiation conditions induced by high-energy neutron, and high fluences of high-flux and low-energy plasma. Tungsten is considered as the most promising material for plasma-facing components (PFCs) in the magnetic confinement fusion devices, due to its high melting temperature, high thermal conductivity, low swelling, low tritium retention, and low sputtering yield. However, some important shortcomings such as the irradiation brittleness and high ductility-brittle transition temperature of pure tungsten limit its application. Focusing on this issue, various W alloys with enhanced performance have been developed. Among them, nanoparticle dispersion strengthening such as oxide particle dispersion-strengthened (ODS-W) and carbide particle dispersion-strengthened (CDS-W) tungsten alloys and W fiber-reinforced W_f/W composites are promising. This chapter mainly reviews the preparation, microstructure, properties, regulation, and service performance evaluation of ODS-W, CDS-W, and W_f/W materials, as well as future possible development is proposed.

Keywords: W alloy, plasma-facing materials, fabrication, performance

1. Introduction

The development of high-performance materials is the major concern for realizing magnetic confinement fusion reactors. The plasma-facing materials (PFMs) work under extreme conditions including high-energy neutron (14.1 MeV) bombardments, severe thermal loads (up to 20 MWm^{-2}), and high fluences of high-flux ($>10^{21} m^{-2} s^{-1}$) and low-energy (<100 eV) hydrogen and helium plasma irradiations [1–3]. The tolerable peak power of the plasma-facing components (PFCs), like the divertor targets, imposes significant restrictions on the design of future fusion reactors such as demonstration (DEMO) reactor or China fusion engineering experiment reactor (CFETR) [4]. Developing advanced materials with improved properties could substantially improve the performance of such PFCs.

Tungsten (W) is a kind of refractory metals that has supreme properties such as high melting temperature, high thermal conductivity, good erosion resistance, low vapor pressure, low swelling, and low tritium retention [1, 5, 6]. These properties are appealing for applications as PFCs in future fusion facilities. However, high brittleness in several regimes including low-temperature embrittlement (relatively high ductile-brittle transition temperature (DBTT)), irradiation embrittlement, and recrystallization embrittlement [7, 8] is one of the main disadvantages, which

limits the engineering application of W alloys, particularly in the nuclear energy fields [3, 9, 10]. The thermal load resistance of material is also intimately linked to the strength and DBTT, because the cracks would initiate when the thermal stress is larger than the ultimate strength of material at temperatures above DBTT or than the yield strength at temperatures below DBTT [11–14]. Currently, the performance of pure W can constrainedly satisfy the ITER servicing condition, but for the CFETR and DEMO with higher working parameters, it is not enough. Therefore, tungsten materials with more excellent mechanical properties, high-temperature stability, and irradiation resistance would be highly desirable for PFCs in future fusion reactors.

For tungsten alloys, decreasing DBTT has been a major goal over recent decades. It is generally understood that the low ductility of tungsten is closely related to their weak grain boundary (GB) cohesion, due to the segregation of interstitial impurities, such as O at GBs [15, 16]. In this sense, methods that purify impurity at GBs should be effective to improve the strength and ductility of tungsten. However at high temperatures (above 1000°C), the strength of pure W decreases significantly [17, 18]. Recent research results indicated that trace active elements, such as Zr, Ti, and Y, in tungsten can react with oxygen and diminish the influence of free oxygen on GBs via forming thermally stable nano-oxide particles and thus purify and strengthen the GBs, raising the stability at high temperature [19–21].

Therefore, several approaches are developed to improve the mechanical properties such as increasing ductility and fracture toughness and decreasing the DBTT. First, tungsten materials with high strength and high thermal stability can be obtained by the dispersing second-phase particles, such as oxides or carbides forming the oxides or carbides and dispersion-strengthened (ODS or CDS) tungsten-based materials [22–30]. Recently, various ODS-W or CDS-W materials with enhanced strength and thermal stability were fabricated and investigated for fusion applications [3, 30]. For example, W-La$_2$O$_3$ and W-Y$_2$O$_3$ showed enhanced strength, high recrystallization temperatures, and high thermal shock resistance [3, 24, 31]. Carbides such as TiC, ZrC, and HfC have much higher melting temperatures than that of the abovementioned oxides and better compatibility with tungsten, which may lead to excellent comprehensive performances in CDS-W. For example, an ultrafine-grained (UFG) W-1.1%TiC fabricated by severe plastic deformation exhibits a very high bending strength up to ~4.4 GPa and appreciable ductility at room temperature (RT) [23]. Zhang et al. [14, 28, 31] developed a bulk W-ZrC alloy with a flexural strength of 2.5 GPa and a strain of 3% at room temperature (RT) and a DBTT of less than 100°C. In addition, the W-ZrC alloy plate can sustain 4.4 MJ/m^2 thermal load without any cracks at RT. The low-energy and high-flux plasma irradiation resistance of this W-ZrC alloy is better than that of W-La$_2$O$_3$, ITER grade pure W, and commercial pure W; the hydrogen retention is also lower than that of ITER grade pure W [31]. W fiber-reinforced W$_f$/W composites also provide a good candidate for PFCs. In this chapter, the comprehensive introduction of the abovementioned materials will be reviewed.

2. Oxide dispersion-strengthened W-based materials

In ODS-W, nanoscaled oxides pin and hinder the migration of grain boundaries and dislocations in tungsten matrix, which improved the mechanical properties such as strength, recrystallization temperatures, and creep resistance. In addition, the dispersion of nanoscaled particles provides a large amount of phase interfaces that could act as sinks for irradiation-induced point defects and thus has the potential in improving the irradiation resistance [29, 31]. For instance, W-(0.3–1.0–2.0)wt%Y$_2$O$_3$ produced by mechanical alloying (MA) and hot isostatic pressing (HIPing) or microwave sintering has fine grains with the grain sizes ranging between 20 and 500 nm and containing a

high density (5.4–6.9×10^{22} m^3) of nanosized Y_2O_3 particles with sizes between 1 and 50 nm [32, 33]. These refined grains and nanosized particles produce high densities of GB/PB interfaces, which generate high strength and a promising radiation resistance. To improve the ductility W-Y_2O_3 materials, different sintering and posttreatments such as spark plasma sintering (SPS) and high-temperature sintering in combination with hot rolling or hot forging deformation were used [34–38]. The performances of these W-Y_2O_3 were investigated as potential plasma-facing materials with respect to microstructures, thermal physical properties, mechanical properties, and thermal shock response when exposed to electron beam bombardment. For SPSed W-Y_2O_3, the tungsten grain exhibits an isotropic microstructure with an average grain size of 3.2 μm; the average of Y_2O_3 particles is about 80 nm [38]. For the sintered W-Y_2O_3 in flowing H_2, Y_2O_3 particles are located at the grain boundaries with a typical bimodal size distribution, i.e., composing of two portions of particles with particle size of ~0.68 and 1.1–1.7 μm, respectively, and the average grain size of tungsten is about 3 μm [34]. The thermal conductivity of deformed W-Y_2O_3 showed nearly 35% and 17% higher values than that of SPSed W-Y_2O_3 at RT and at 1473 K, respectively [34]. The tensile tests showed that the deformed W-Y_2O_3 is ductile in the investigated temperature range of 673–1273 K with the total elongation between 4% and 10%. Three-point bending tests indicated that the deformed W-Y_2O_3 had a better mechanical strength and toughness. The determination of thermal shock response revealed a superior thermal shock resistance of the hot rolled W-Y_2O_3 [34]: no cracks but only surface roughening was found on the loaded surface after 100 shots at 0.6 GW/m^2 for a pulse duration of 1 ms. Besides, the melting and recrystallization behaviors of deformed W-Y_2O_3 were less obvious than those of SPSed W-Y_2O_3 [34]. The discrepancy in thermal shock response between the two materials and in particular the superiority of deformed W-Y_2O_3 agrees well with the results that the better the thermophysical and mechanical properties, the better the thermal shock resistances. The high-energy-rate forging may significantly improve mechanical properties of W-Y_2O_3 materials [35]. It is indicated that needlelike grains ranging from a few to more than 50 μm in forged W-Y_2O_3 lead to the improved mechanical properties [35]. A detectable plastic deformation (TE = 2.9%) associated with work hardening occurs at 100°C, and the ultimate tensile strength of this forged W-Y_2O_3 material increases drastically to 1040 MPa.

For swaging deformed W-Y_2O_3, tungsten grains are round bar in shape [38]. The average diameter and length of tungsten grain in swaged W-Y_2O_3 are 4.6 and 26.7 μm, respectively, corresponding to an aspect ratio of about 6:1. The tensile results have shown that it is a brittle fracture until above 250°C and its strength is also smaller than that of the high-energy-rate forging ones [35], which implies that bimodal interfaces (in forged ones) are more in favor of strengthening and ductility. Therefore, it is important to notice that again the microstructure design, here from hot forging, is at least as important as the ODS effect. Although the addition of Y_2O_3 can produce PB interfaces and control GB interfaces, it cannot reduce the detrimental impurities of oxygen. Xie et al. [21] added Zr element into W-Y_2O_3 to absorb free oxygen at GBs to form Y-Zr-O particles, and at the same time, the particle size of Y-Zr-O can be further reduced. Because of the improved PB/GB interfaces by Zr, the strength and plasticity of this W-Zr-Y_2O_3 increase further on the base of W-Y_2O_3.

3. Carbide dispersion-strengthened tungsten-based materials

As compared with the oxides' strengthening phases, the carbides, such as TiC, ZrC, and HfC, have much higher melting temperatures and better compatibility with tungsten, which may lead to excellent comprehensive performance. Kurishita et al. reported ultrafine-grained (UFG) W-TiC alloys which showed increased

mechanical properties and better irradiation resistance [22, 39, 40]. These favorable properties of W-TiC alloys imply the potential of other carbide dispersion-strengthened tungsten materials with fine microstructures.

Among these carbide-strengthened phases, ZrC and TaC have high melting temperatures of 3540°C and 3900°C, respectively. It's worth mentioning that the lattice match of $d_{(200)ZrC} \approx d_{(110)W} \approx 0.221$ nm might introduce coherent PB interface between ZrC phase and W matrix, which will significantly increase PB cohesion. In addition, ZrC as an oxygen getter can react with oxygen to form stable Zr-C-O or ZrO_2 particles at GBs, purifying GB interface, and thus is beneficial to improve the GB cohesion and enhance the low-temperature ductility of tungsten.

Fan et al. [27, 41] fabricated W-ZrC material by high-temperature sintering in hydrogen atmosphere using W-ZrC composite powders prepared by sol-heterogeneous precipitation-spray drying-thermal reduction. The relative density of their W-(0, 1, 2, 3, 4)%ZrC samples is in the range of 98.5–99.7%. They found that the addition of ZrC could refine tungsten grains and improve the strength. The grain size of W-3%ZrC (10~15 μm) is much smaller than that of pure W (~100 μm), and the ZrC particles are micron-sized; most of them are distributed at grain boundaries. Xie et al. [42, 43] fabricated a series of W-(0, 0.2, 0.5, 1.0)%wtZrC with an average grain size which ranges from 2.7 to 4.2 μm by using mechanical alloy and SPS. The ultimate tensile strengths (UTS) of SPS pure W and W-(0.2, 0.5, 1.0)%ZrC at 700°C are 337, 419, 535 and 749 MPa, respectively, suggesting enhancements in strength by adding a small amount of ZrC nanoparticles. The strength of W-0.5%ZrC (W-0.5ZrC) is over 50% higher than that of pure W. Meanwhile, the ductility could also be effectively improved by the ZrC addition.

On the basis of composition optimization, Xie et al. [28] fabricated bulk W-0.5wt%ZrC plates with a thickness of 8.5 mm, which are suitable for engineering application. This material exhibits very good mechanical properties. At RT, this bulk W-0.5ZrC plate exhibits a high bending stress of 2.5 GPa as well as a flexural strain of 3%, which is much higher than those of the hot rolled W, HIPed pure W [44], and W-1.0Y$_2$O$_3$ [45] and close to those of the severely deformed W-TiC alloys [46]. The DBTT is about 100°C (see **Figure 1** and **Table 1**), which is much lower than that of reported bulk W alloys and several other tungsten materials [31, 47]. At temperatures above 150°C, the W-0.5ZrC plates can be bent to a high flexural strain of 15% (limited by the machine) without any crack.

Figure 1e shows the engineering stress-stain curves of the W-0.5ZrC alloy tested at various temperatures along rolling direction (RD). At 100°C, the W-0.5ZrC plate exhibits obvious tensile deformation with a TE~3% and an UTS value up to 1.1 GPa. With the increase of the test temperature to 200°C, the TE increases to 14.2%, and the UTS maintains as high as ~1 GPa. At a higher testing temperature of 500°C, the UTS is still very high (583 MPa), and the TE increases up to 41%. The rolled W-0.5ZrC showed both higher strength and ductility than that of the rolled W-0.5TiC [48] and rolled W-0.5TaC [49], which were fabricated following a similar process. The W-3%Re and K-doped W-3%Re show ductility at 100°C, which is comparable with W-0.5ZrC plate, while their tensile strength values (<1000 MPa) are lower than that of W-0.5ZrC plate (1058 MPa) [50]. As compared with Plansee ITER specification W (IGP), AT&M ITER specification W (CEFTR), W-1wt%TiC (W1TiC), W-2wt%Y$_2$O$_3$ (W2YO) from Karlsruhe Institute of Technology at Germany, and fine-grained W (FG) from the Institute of Plasma Physics at Czech Republic, W-0.5ZrC exhibits the highest tensile strength and lower DBTT [51], as shown in **Figure 2**.

For PFCs, the transient heat load events such as major plasma disruptions, edge-localized modes (ELMs), and vertical displacement events (VDEs) are serious issues [11], which may lead to a significant temperature rise and high thermal
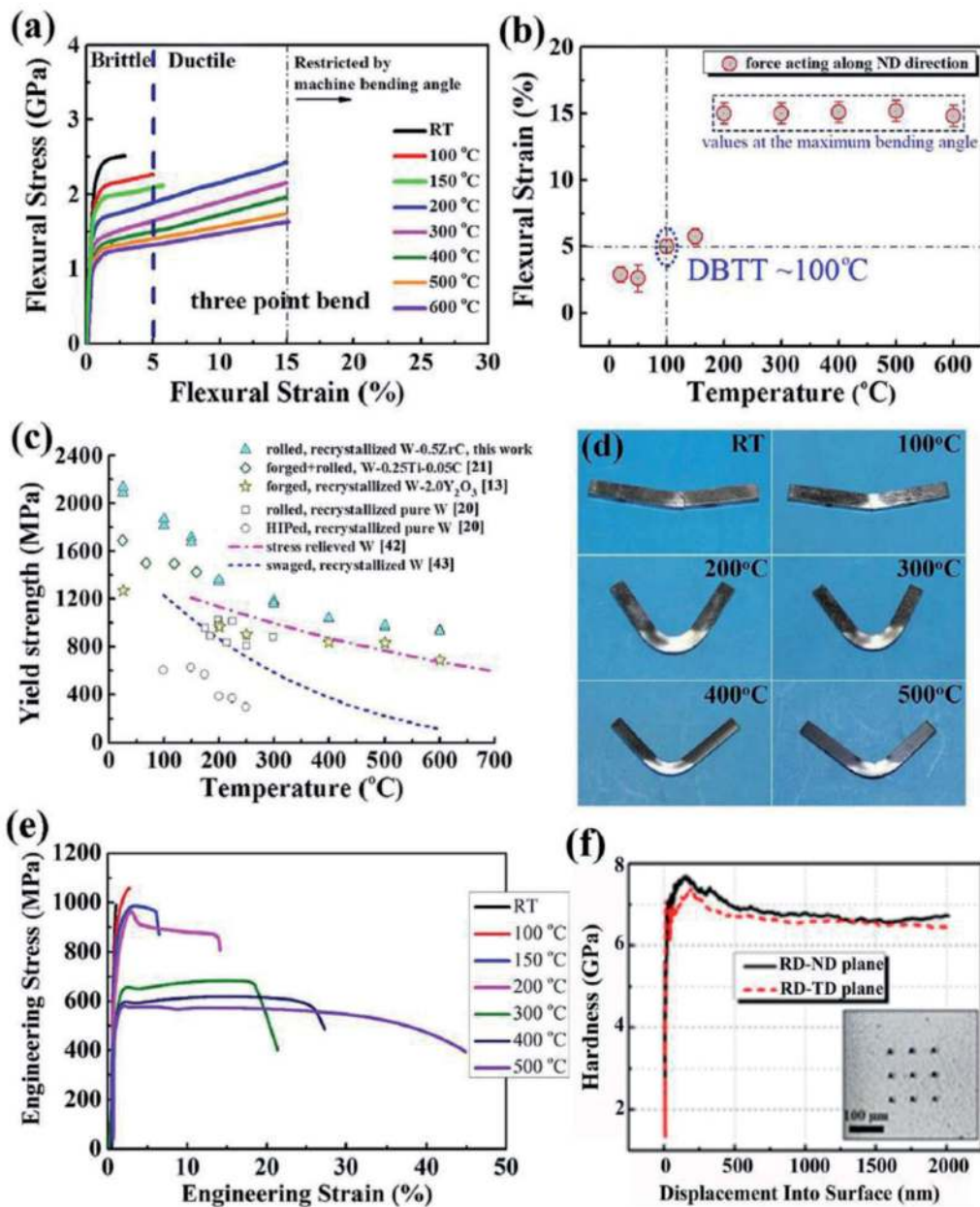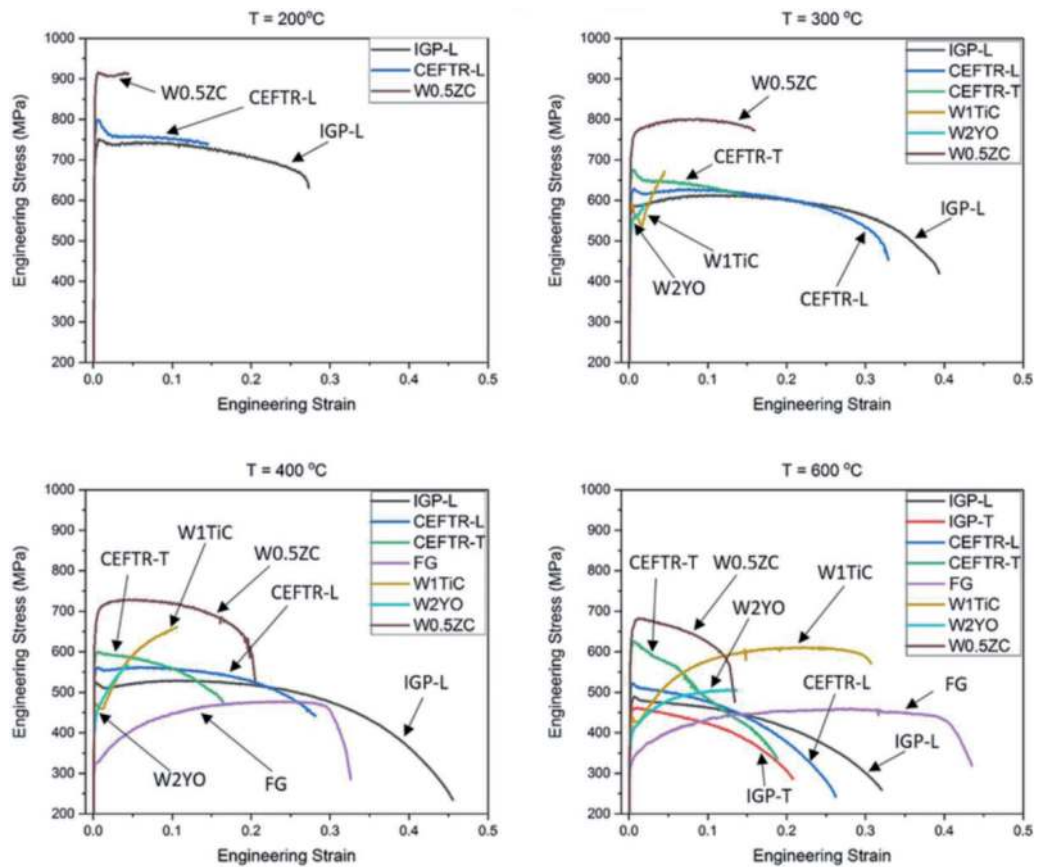
Figure 1.
Mechanical properties of W-0.5ZrC alloy: (a) flexural stress-strain curves tested at various temperatures (note that values larger than a flexural strain of 15% is not accurate due to the limited bending angle of the machine). (b) Flexural strain of W-0.5ZrC at various test temperatures. (c) Temperature dependence of the yield strength (YS) by 3-point bending test in comparison with available literature data. (d) Optical images of 3-point bending specimens tested at various temperatures. (e) Tensile engineering stress-strain curves of W-0.5ZrC at different temperatures. (f) Hardness in different planes of W-0.5ZrC tested by nanoindenter [28].

stresses in PFCs. The abrupt high temperature during transient events can lead to material recrystallization, grain growth, surface melting, and droplet ejection. The high thermal stresses can lead to cracking, fatigue fracture, and fatal destruction of the PFCs. Therefore, the thermal shock resistance of PFCs is closely related to their mechanical properties. Intuitively, high strength could resist a relatively high stress induced by thermal shocks to prohibit the cracking formation, while good plasticity/ductility is in favor of releasing the stress via plastic deformation rather than cracking. That is to say, a higher strength and better low-temperature ductility would lead to the better thermal shock resistance [28, 31, 52].

Materials/size	Working process	DBTT (K)	Dimension (mm)	Methods
W-0.5ZrC (8.5 mm thick plate)	Rolling	373	2 × 2 × 20	3 PB
Pure W (0.1 mm thick foil)	Rolling + joining	373	4 × 15 × 33	Charpy
Pure W (10 mm thick plate)	Rolling	473	2 × 4 × 20	3 PB
Pure W (4 mm thick)	HIP	473	2 × 3.3 × 20	3 PB
Pure W	Injection molding	1173	3 × 4 × 27	Charpy
W-2Y$_2$O$_3$ (2 mm thick, Φ 95 mm)	Hot forging	473	2 × 2 × 25	3 PB
W-1%Y$_2$O$_3$	Injection molding	1273	3 × 4 × 27	Charpy
W-0.2Zr–1.0Y$_2$O$_3$ (Φ 9 mm rod)	Swaging	423	2 × 3.3 × 20	3 PB
W-0.25Ti–0.05C (1 mm thick plate)	Rolling	260	1 × 1 × 20	3 PB
W-0.2TiC (1 mm thick)	Forging + rolling	440	1 × 1 × 20	3 PB
W-0.5TiC	HIP + forging	484	1 × 1 × 20	3 PB
WL10	Swaging + rolling	973	10 × 10 × 55	Charpy

Table 1.
DBTT of the rolled W-0.5ZrC and several reported W materials [31].

Figure 2.
The tensile stress of various W materials [51].

Figure 3 shows the thermally loaded surfaces of rolled W-0.5ZrC after exposure to single shot with a pulse length of 5 ms using an electron beam. No cracks or melting were observed on the samples when tested at an absorbed power
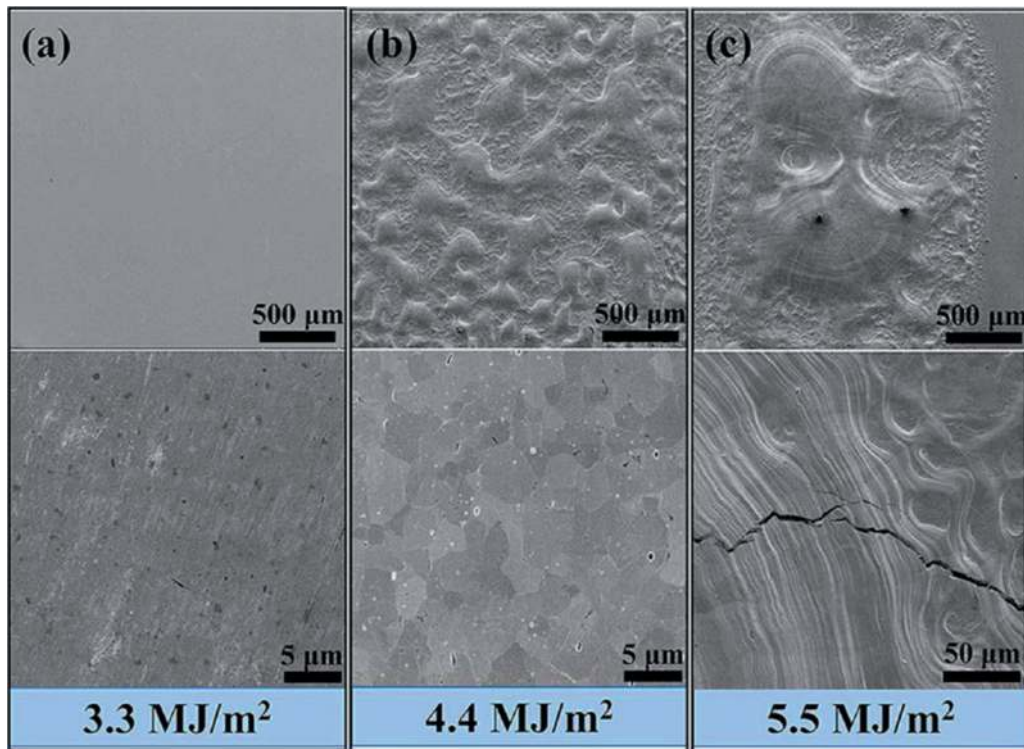
Figure 3.
The SEM images of sample surfaces after exposure to thermal shocks with a pulse duration of 5 ms. (a) 3.3 MJ/
m^2 (0.66 GW/m^2), (b) 4.4 MJ/m^2 (0.88 GW/m^2), and (c) 5.5 MJ/m^2 (1.1 GW/m^2) [28]. No cracks were found
at 0.88 GW/m^2 although the sample surface melted and the cracking threshold is 0.88~1.1 GW/m^2.

density (APD) of 0.66 GW/m^2 as shown in **Figure 3a**. Still no crack at an APD of
0.88 GW/m^2 but surface melting was observed as shown in **Figure 3b**. The results
suggest that the melting threshold of the rolled W-0.5ZrC is ~0.88 GW/m^2.
When the APD increased to 1.1 GW/m^2 (**Figure 3c**), both cracks and melting were
found on the sample surface, indicating a crack threshold of 0.88–1.1 GW/m^2. For
comparison, the cracking thresholds of previously reported tungsten materials
like sintered W, chemical vapor deposition (CVD) W, deformed W, potassium-
doped W (W-K), and W-La$_2$O$_3$ alloys [53–57] were summarized in **Table 2**.
These results further indicate the excellent thermal shock resistance of the rolled
W-0.5ZrC.

During the thermal shock, the materials are heated and undergo thermal
expansion, which is restricted by the colder surrounding material, causing
compressive stress [53]. If the compressive stress exceeds the yield strength of the
tested tungsten material, plastic deformation would occur because of the mate-
rial plastic at high temperatures. During the cooling stage, the thermally loaded
area shrinks, and the compressive stress is converted into a tensile stress [53].
Thus the cracks would form if the stress exceeds the ultimate tensile strength
of the materials. Therefore, the excellent thermal shock resistance of the rolled
W-0.5ZrC seems reasonable, because it has high strength, a lower DBTT, and
good plasticity.

Thermal fatigue behaviors of the as-rolled and recrystallized W-0.5ZrC alloys
were investigated by repetitive thermal shocks (100 shots in total) with a pulse
duration of 1 ms at RT [14]. The cracking thresholds for the as-rolled and recrystal-
lized W-0.5ZrC are 0.22–0.33 GW/m^2, which is comparable to that of ultrahigh-
purity W but lower than that of W-5%Ta [52]. It's reported that at higher base
temperatures, tungsten materials tend to exhibit enhanced resistance to thermal

Alloys	State	Crack thresholds (GW/m^2)
W-0.5ZrC	Swaged	0.22–0.44
W-0.5ZrC	Rolled	0.88–1.1
CVD W	—	0.28–0.33
W	As-sintered	0.33–0.55
W	Recrystallized	<0.33
Rolled W	As-rolled	0.44–0.66
Forged W	Stress relieved/ recrystallized	0.15–0.33
W-K alloy	Swaged + rolled	0.44–0.66
W-Y$_2$O$_3$	—	0.6
WL10	Rolled	<0.22
W-TiC	—	0.33

Table 2.
Comparison of W-ZrC alloys and some tungsten materials after single thermal shock loads at RT with a pulse duration of 5 ms [31].

shocks because of the increased ductility of materials [13]. Nevertheless, there are still no results of the thermal fatigue behavior of the rolled W-0.5ZrC at higher base temperatures, which would be investigated in the near future.

The irradiation resistance to plasma is another key property for PFCs. The PFCs in fusion reactors suffer from the high-flux (about 10^{24} m^{-2} s^{-1}) low-energy plasma irradiation, which would cause bubbles and erosion phenomena on the surface of PFCs, and lead to the degradation of performances. More badly, the excessive erosion dusts will extinguish the burning plasma. Therefore, the less the erosion, the better.

Liu et al. [58] studied the irradiation damage of several newly developed tungsten materials including pure tungsten, CVD-W, W-0.5ZrC, W-1.0wt.%Y$_2$O$_3$, W-1.0vol.%Y$_2$O$_3$, and W-1.0La$_2$O$_3$ under low-energy He plasma neutral beam. **Figure 4** shows the surface and cross-sectional morphologies of irradiation-modified layers on the abovementioned tungsten materials after high fluences (10^{26} ions/m^2) of low-energy helium plasma irradiation [58]. After 220 eV He-ion irradiation at 900°C, all samples showed pinhole features on the irradiated surface, while in the case of 620 eV He-ion irradiation at 1000°C, the pinhole surface evolved into coral-like features except for the W-0.5ZrC alloy which retains the pinhole feature [58]. This result indicates the good resistance of W-0.5ZrC alloy to He-ion irradiation. The fine-grained W-0.5ZrC alloy has abundant GBs and PBs which all provide nucleation sites for He atom aggregation and thus reduce the concentration of He, thus hindering the growth of He bubbles and mitigating the evolution from pinhole to coral-like structures. The thickness of modified layers on the surface of tungsten materials was measured and plotted in **Figure 5**, in which W-La, W-Y1, and W-Y2 represent W-1wt.%La$_2$O$_3$, W-1wt.%Y$_2$O$_3$, and W-1vol.%Y$_2$O$_3$, respectively. The thickness of modified layers on W-0.5ZrC is much lower than that of pure W, W-La, and W-Y1, implying its better resistance to plasma irradiation and erosion [58].

Liu et al. [58] also studied the evolution of morphology and thermal-mechanical properties of pure W, CVD-W, and W-0.5ZrC alloys after pure H beam and H/ He mixed beam irradiation using the neutral beam facility GLADIS (Max Planck Institute for Plasma Physics, Germany). It is found that just roughness occurred on all W material surfaces after H irradiation, while a mixture of 6% He resulted in pinhole structures, indicating the crucial factor of He irradiation for the surface modification. The unexposed and pre-irradiated CVD-W and W-0.5ZrC were then
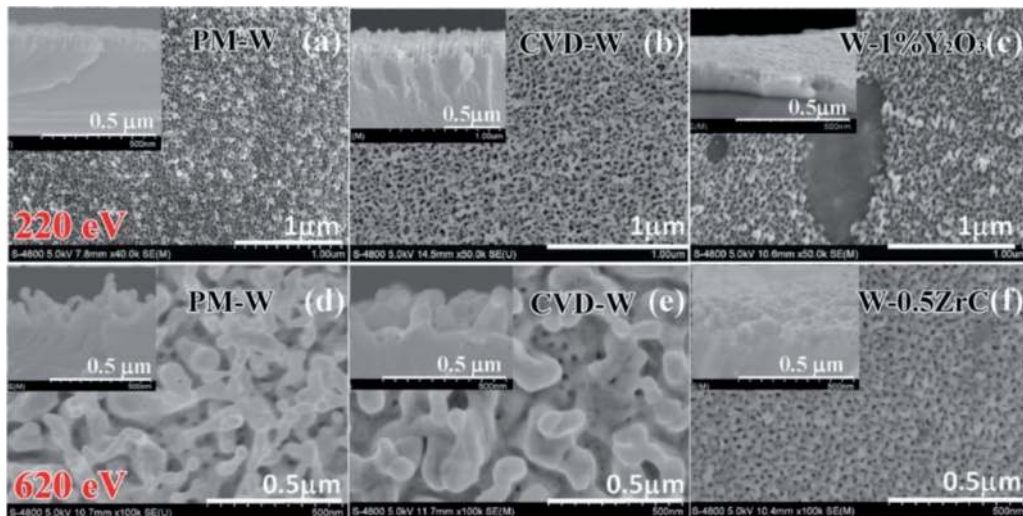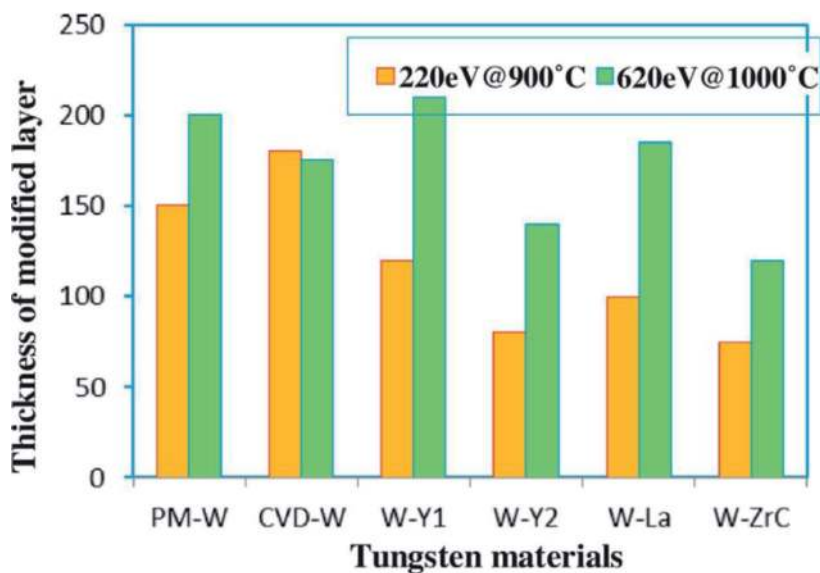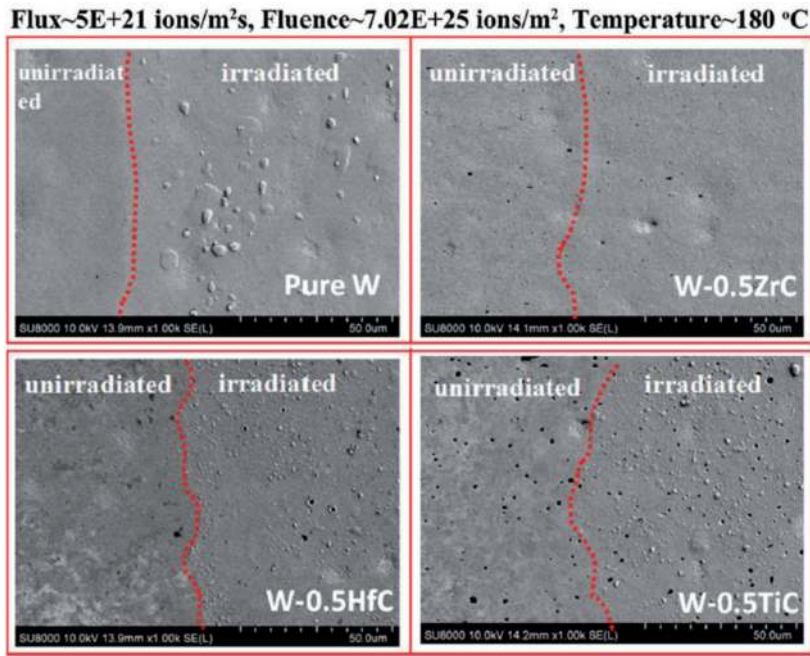
Figure 4.
The surface morphologies of (a) pure W, (b) CVD-W, (c) W-1.0%Y$_2$O$_3$ irradiated by 220 eV He$^+$ at about 900°C and (d) pure W, (e) CVD-W, and (f) W-0.5ZrC irradiated by 620 eV He$^+$ at 1000°C to a same fluence of 1 × 10^{26} atoms/m^2 [58]. The insets of (a)–(f) show the corresponding cross-sectional morphologies of irradiation-modified layer in each sample.

loaded repeatedly by thermal shocks through an electron beam with a 1 ms pulse and 100 cycles. The cracking threshold of unexposed CVD-W is about ~0.22 GW/m^2, a little lower than that of W-0.5ZrC. Pre-irradiation by H only seems to have less effect on the critical cracking thresholds, while pre- irradiation by H/He mixed beam significantly reduces the cracking thresholds [58].

The effects of deuterium (D) plasma irradiation on the microstructure of W-ZrC were also investigated. Several CDS-W materials, including rolled W-0.5ZrC [28], W-0.5HfC [30], W-0.5TiC [48], as well as pure W, were subjected to D plasma irradiation in the linear plasma device of simulation for tokamak edge plasma (STEP) [59]. **Figure 6** shows the morphologies of these materials after exposing to D plasma irradiation under a same condition

Figure 5.
Thickness of modified layers in various tungsten materials under the He+ irradiation of 220 eV at 900°C and 620 eV at 1000°C [58].
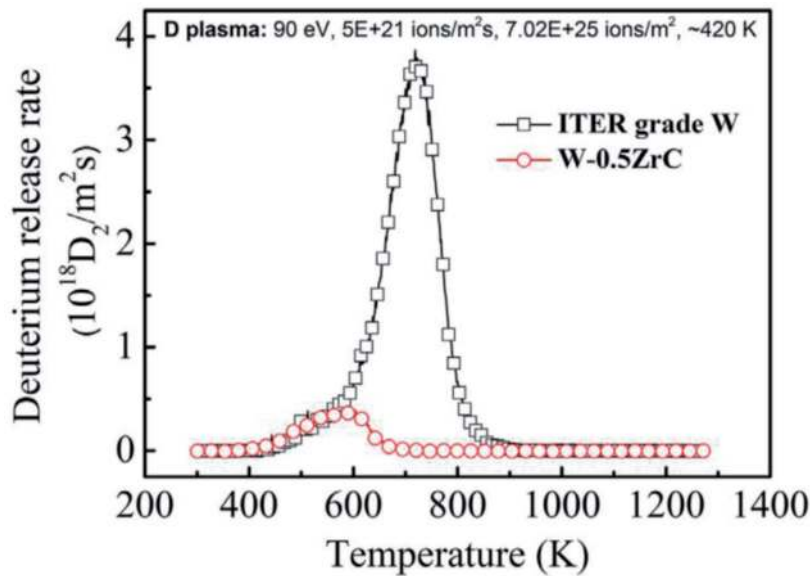
Figure 6.
Surface morphologies of pure W, rolled W-0.5ZrC, W-0.5HfC, and W-0.5TiC irradiated by D plasma. [31].

(D^+ energy ~90 eV, flux ~5 × 10^{21} ions/m^2 s, fluence~7.02 × 10^{25} ions/m^2, temperature ~180°C) [31]. Surface swelling and a high density of large bubbles with size ranging from 1 to 10 μm were found on the surface of the pure W. On the surface of W-0.5HfC and W-0.5TiC, the bubble size was much smaller (less than 1 μm). In the case of W-0.5ZrC, only blisters (about 100 nm) were observed, despite the high blister density. These results further indicate the increased resistance to bubble formation to D plasma irradiation. The enhanced irradiation resistance may come from the fine grains and homogeneously dispersed nanoscaled particles in the rolled W-0.5ZrC, which provide a large number of GB and PB interfaces that act as effective sinks for irradiation-induced defects [60–62].

The hydrogen isotopes especially tritium retention behaviors in PFCs are also an important issue, which has an impact on the tritium fueling and the safety of fusion reactors and has not been completely understood. The hydrogen isotope retention behaviors of W-ZrC alloy were investigated through plasma irradiation and thermal desorption spectrum (TDS) analysis. The D plasma irradiation was carried out in the STEP device [59]. Rolled pure W and W-0.5ZrC were exposed to low-energy high-flux deuterium plasma under the same condition (D^+ energy~ 90 eV, flux ~5 × 10^{21} ions/m^2 s, fluence~7.02 × 10^{25} ions/m^2, temperature 400 K). After irradiation, the TDS results have shown that the rolled W-0.5ZrC exhibits much lower hydrogen retention than that of pure W as shown in **Figure** 7. This result indicates that the hydrogen retention in W-ZrC is not increased although they contain the Zr element, because the Zr element exists in the form of stable carbide or oxide particles. Both the rolled W-0.5ZrC and pure W had a desorption peak at temperature around 560°C, and the peak intensity of W-0.5ZrC is much lower than that of pure W.

The above performance is closely related to the microstructure of the rolled W-0.5ZrC. The detailed microstructures show the coexistence of multi-scale interfaces in the rolled W-0.5ZrC plate. From the outer to inner space, in the first layer along the rolling direction, the average length of mother grains is about

Figure 7.
TDS results of pure W and W-0.5ZrC after 90 eV high-flux (~5 × 10²¹ ions/m² s) D plasma irradiation to a fluence of 7.02 × 10²⁵ ions/m² at 400 K [31].

10 μm, and the width is about 1~3 μm, which is the micrometer scale GB interface [28]. Prolonged mother grains come from the multistep rolling deformation. In the second layer, there are equiaxed sub-grains in the matrix with average size of about 1 μm, which could be considered to the sub-micrometer scale GB interfaces. The sub-grains can be attributed to the deformation and dynamic recrystallization resulting from the precise control of rolling parameters [28]. For the third layer, most of the nanoscaled particles disperse in tungsten grain interior. The size distributions of the particles indicate that most particles located in W grains have an average size of 51 nm, while parts of particles at W GBs show bimodal distribution which contains relatively small particles with an average particle size of 60 nm ranging from 40 to 200 nm and a small fraction of large particles with an average particle size of 385 nm ranging from 250 to 400 nm [28]. It is worth pointing out that the small particles at GBs are dominantly ZrC, while the large particles are W-Zr-C-O complexes, which eliminate the free O at GBs and purifying GB interfaces. Therefore, the third layer interface is the nanoscale or sub-micrometer scale interface. The intuitive magnifying HRTEM of PBs shown in **Figure 8a–e** exhibits a perfect coherent structure interface between W matrix and ZrC dispersoids. This atomic ordered interface could pin and accumulate dislocations and thus effectively raise the strength and simultaneously improve the ductility of alloys.

The multi-scaled interface structure is in favor of irradiation resistance and decreases the retention of hydrogen. Mother grain boundaries may provide rapid diffusion paths for H and its isotope [63], and thus H could easily diffuse to the surface of the specimen even at a relatively low temperature. Thus a large fraction of D atoms may escape from the W-0.5ZrC during the D plasma irradiation at 400 K, leading to low retention of D in materials. At the same time, the fine sub-grains increase the GB interface density, and the nanosized particles create a high density of PB interfaces, which can absorb interstitial defects and then annihilate nearby vacancies by re-emitting the interstitial atoms back into the grain, thus improving the ability of irradiation resistance of W-0.5ZrC alloy.
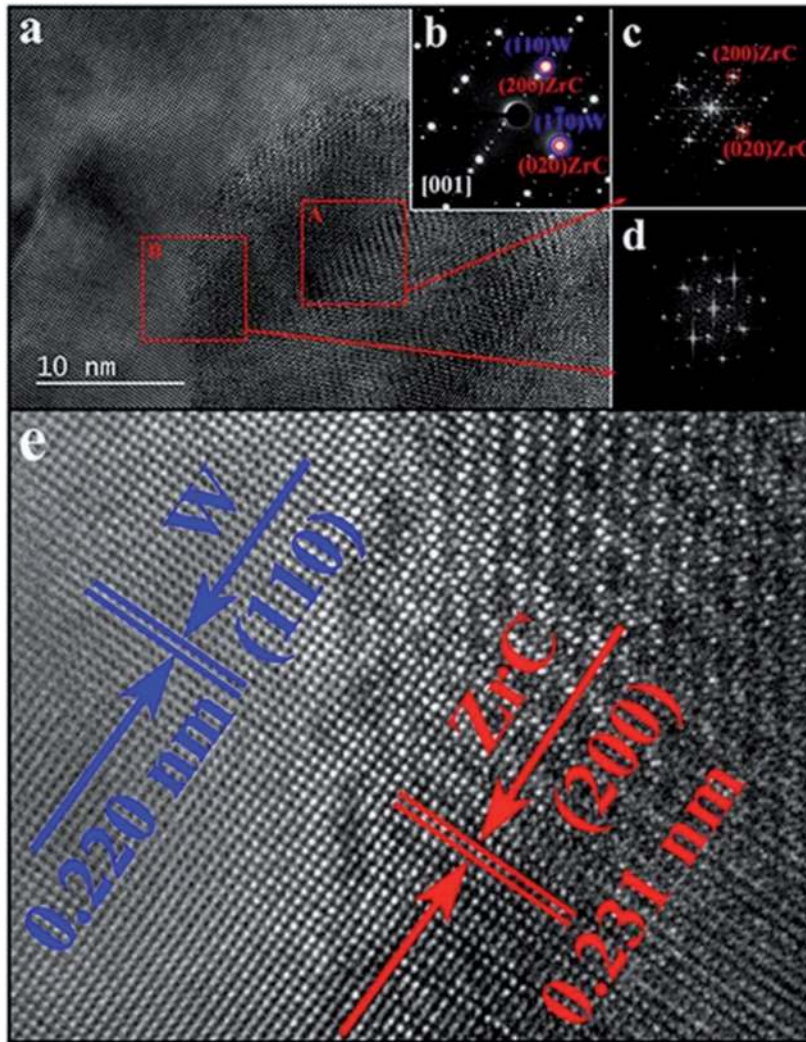
Figure 8.
(a) HRTEM image of W matrix and ZrC phase (intragranular) as viewed along [001]. (b) The SAEDP revealing the particle with a face-centered cubic structure. (c) Fast Fourier transform (FFT) pattern of selected red square area A on ZrC. (d) FFT pattern of selected red square area B at interface area between W and ZrC. (e) It is clear that the particle-matrix phase boundaries have a coherent structure like that shown in high magnification [28].

4. W fiber-reinforced W_f/W composites

Since a decade, a promising method of toughening tungsten composites using tungsten fiber reinforcement has been actively pursued, namely, tungsten fiber-reinforced tungsten (W_f/W) composites [64–72]. However, in the bared W_f/W, the interface is not obvious due to the chemical reaction between W_f and W matrices, so the reinforcing effect is not ideal. Therefore, in this material concept, tungsten fibers are embedded in a tungsten matrix where a proper interface has to be introduced to prevent a chemical reaction between the two components. The increase in toughness is achieved through a couple of non-plastic energy dissipation mechanisms such as matrix cracking and interfacial debonding followed by frictional sliding/pullout of the fibers, while the primary crack is bridged by mostly elastically deforming fibers [65, 73]. To maximize the energy dissipation, the interfaces need to be engineered by coating which can withstand thermal exposure during service. Du et al. [65] investigate the thermal stability of the various kinds of coated interfaces for W_f/W composites: Cu/W multilayer, Er/W multilayer, ZrO_x/W bilayer, ZrO_x/Zr multilayer,

and C/W dual layer. These coatings were selected for interface engineering with which one utilizes energy dissipation by controlled interfacial debonding and sliding achieving apparent toughness. Regarding the effect on the interfacial properties, the fracture energy of the Er/W multilayer and the ZrO_x/Zr multilayer was affected by less than 10%, while it increased by 40% for the ZrO_x/W bilayer. Therefore, the ZrO_x/W bilayer interface is the best choice for W_f/W composite. The single direction of W fibers can enhance the fracture energy of tungsten matrix once the extrinsic toughening mechanisms of fiber pullout and plastic deformation were triggered, but they will lead to the obvious anisotropy of mechanical properties [73]. Lama et al. [74] use woven tungsten wire meshes as reinforcement in the composites (wire diameter, 127 μm; distance between wires, 1 mm), which avoided the anisotropy induced by single direction of W fibers. In addition, a stable interfacial coating zirconia film (ZrO_x) was deposited on the meshes by magnetron sputtering. The zirconia coating could survive the heat loads without any notable damage or overall cracking. The coating thickness remained mostly unchanged. Therefore, under the extreme environment, the zirconia coating interfaces are stable, which is in favor of reinforcing the W_f/W composites [75, 76].

5. Summary and outlook

The improvements in different aspects of tungsten have been enriching the knowledge base and help to show the way to high-performance tungsten materials for fusion applications. Nevertheless, to satisfy the requirements of PFCs in future fusion facilities, the performances of tungsten materials need to be further improved, which may be achieved through several approaches as follows. Firstly, microstructure optimization includes the size and shape of tungsten grains and the size, distribution, and the number density of second-phase particles in tungsten-based materials. For ODS-W or CDS-W, the size of strengthening particles is not small enough; if second-phase particles could be further refined, e.g., to 10 nm or even smaller, more favorable particle-matrix interfaces would be constructed, and thus mechanical properties, resistance to thermal loads, and irradiation might be further improved. Secondly, to reduce the DBTT and improve the low-temperature ductility, the content of detrimental interstitial impurities (i.e., O, N) should be as low as possible. For the W_f/W composites, the interface is still a weak point and needs to be further optimized.

For the materials used in fusion reactors, the synergistic effects of multi-loadings including high thermal loads, high-flux H/He plasma etching, and neutron irradiation may lead to much more severe degradation of properties. Therefore, the synergistic effects of high heat loads, low-energy high-flux plasma etching and neutron irradiation, and transmutation elements on the microstructures and properties of tungsten materials need to be systematically investigated in the near future, which is necessary to evaluate the performance of the tungsten materials more accurately, and the corresponding database for the performance of tungsten materials should be established.

Acknowledgements

Author details

Tao Zhang[1*], Zhuoming Xie[2], Changsong Liu[2] and Ying Xiong[3]

1 School of Physics and Electronic Engineering, GuangZhou University, GuangZhou, China

2 Institute of Solid State Physics, Chinese Academy of Sciences, Hefei, China

3 State Key Laboratory of Environment-Friendly Energy Materials, Southwest University of Science and Technology, Mianyang, China

*Address all correspondence to: zhangtao@issp.ac.cn

IntechOpen

References

[1] Knaster J, Moeslang A, Muroga T. Materials research for fusion. Nature Physics. 2016;**12**:424-434

[2] Raffray AR, Nygren R, Whyte DG, et al. High heat flux components—Readiness to proceed from near term fusion systems to power plants. Fusion Engineering and Design. 2010;**85**:93-108

[3] Rieth M, Dudarev SL, de Vicente SMG, et al. Recent progress in research on tungsten materials for nuclear fusion applications in Europe. Journal of Nuclear Materials. 2013;**432**:482-500

[4] Linsmeier C, Rieth M, Aktaa J, et al. Development of advanced high heat flux and plasma-facing materials. Nuclear Fusion. 2017;**57**:092007

[5] Bolt H, Barabash V, Krauss W, Linke J, Neu R, Suzuki S, et al. Materials for the plasma-facing components of fusion reactors. Journal of Nuclear Materials. 2004;**329**:66-73

[6] Smid I, Pacher HD, Vieider G, Mszanowski U, Igitkhanov Y, Janeschitz G, et al. Lifetime of Be-, CFC-and W-armoured ITER divertor plates. Journal of Nuclear Materials. 1996;**233**:701-707

[7] Kurishita H, Arakawa H, Matsuo S, et al. Development of nanostructured tungsten based materials resistant to recrystallization and/or radiation induced embrittlement. Materials Transactions. 2013;**54**:456-465

[8] Norajitra P, Boccaccini LV, Gervash A, et al. Development of a helium-cooled divertor: Material choice and technological studies. Journal of Nuclear Materials. 2007;**367**:1416-1421

[9] Wurster S, Baluc N, Battabyal M, et al. Recent progress in R&D on tungsten alloys for divertor structural and plasma facing materials. Journal of Nuclear Materials. 2013;**442**:S181-S189

[10] Byun TS, Li M, Cockeram BV, Snead LL. Deformation and fracture properties in neutron irradiated pure Mo and Mo alloys. Journal of Nuclear Materials. 2008;**376**:240-246

[11] Garkusha IE, Landman I, Linke J, Makhlaj VA, Medvedev AV, Malykhin SV, et al. Performance of deformed tungsten under ELM-like plasma exposures in QSPA Kh-50. Journal of Nuclear Materials. 2011;**415**:S65-S69

[12] Linke J, Loewenhoff T, Massaut V, Pintsuk G, Ritz G, Rodig M, et al. Performance of different tungsten grades under transient thermal loads. Nuclear Fusion. 2011;**51**(7):073017

[13] Liu X, Lian YY, Chen L, Chen ZK, Chen JM, Duan XR, et al. Experimental and numerical simulations of ELM-like transient damage behaviors to different grade tungsten and tungsten alloys. Journal of Nuclear Materials. 2015;**463**:166-169

[14] Xie ZM, Miao S, Liu R, Zeng LF, Zhang T, Fang QF, et al. Experimental and numerical simulations of ELM-like transient damage behaviors to different grade tungsten and tungsten alloys. Journal of Nuclear Materials. 2017;**496**:41-53

[15] Kurishita H, Matsuo S, Arakawa H, et al. Current status of nanostructured tungsten-based materials development. Physica Scripta. 2014;**T159**:014032

[16] Liu R, Xie ZM, Zhang T, Fang QF, Wang XP, Hao T, et al. Mechanical properties and microstructures of W-1% Y_2O_3 microalloyed with Zr. Materials Science and Engineering: A. 2016;**660**:19-23

[17] Aguirre MV, Martin A, Pastor JY, Llorca J, Monge MA, Pareja R. Mechanical Behavior of W-Y_2O_3 and W-Ti Alloys from

25°C to 1000°C. Metallurgical and Materials Transactions A: Physical Metallurgy and Materials Science. 2009;**40**(10):2283-2290

[18] Song GM, Wang YJ, Zhou Y. Thermomechanical properties of TiC particle-reinforced tungsten composites for high temperature applications. International Journal of Refractory Metals and Hard Materials. 2003;**21**:1-12

[19] Xie ZM, Liu R, Fang QF, Zhou Y, Wang XP, Liu CS. Spark plasma sintering and mechanical properties of zirconium micro-alloyed tungsten. Journal of Nuclear Materials. 2014;**444**:175-180

[20] Liu R, Xie ZM, Hao T, Zhou Y, Wang XP, Fang QF, et al. Fabricating high performance tungsten alloys through zirconium micro-alloying and nano-sized yttria dispersion strengthening. Journal of Nuclear Materials. 2014;**451**:35-39

[21] Xie ZM, Liu R, Zhang T, Fang QF, Liu CS, Liu X, et al. Achieving high strength/ductility in bulk W-Zr-Y$_2$O$_3$ alloy plate with hybrid microstructure. Materials and Design. 2016;**107**:144-152

[22] Kurishita H, Amano Y, Kobayashi S, Nakai K, Arakawa H, Hiraoka Y, et al. Development of ultra-fine grained W–TiC and their mechanical properties for fusion applications. Journal of Nuclear Materials. 2007;**367**:1453-1457

[23] Kurishita H, Matsuo S, Arakawa H, Sakamoto T, Kobayashi S, Nakai K, et al. Development of re-crystallized W–1.1% TiC with enhanced room-temperature ductility and radiation performance. Journal of Nuclear Materials. 2010;**398**:87-92

[24] Rieth M, Dafferner B. Limitations of W and W–1% La$_2$O$_3$ for use as structural materials. Journal of Nuclear Materials. 2005;**342**:20-25

[25] Yar MA, Wahlberg S, Bergqivist H, Salem HG, Johnsson M, Muhammed M. Spark plasma sintering of tungsten–yttrium oxide composites from chemically synthesized nanopowders and microstructural characterization. Journal of Nuclear Materials. 2011;**412**:227-232

[26] Yar MA, Wahlberg S, Bergqvis H, Salem HG, Johnsson M, Muhammed M. Chemically produced nanostructured ODS–lanthanum oxide–tungsten composites sintered by spark plasma. Journal of Nuclear Materials. 2011;**408**:129-135

[27] Fan JL, Han Y, Li PF, Sun ZY, Zhou Q. Micro/nano composited tungsten material and its high thermal loading behavior. Journal of Nuclear Materials. 2014;**455**:717-723

[28] Xie ZM, Liu R, Miao S, Yang XD, Zhang T, Wang XP, et al. Extraordinary high ductility/strength of the interface designed bulk W-ZrC alloy plate at relatively low temperature. Scientific Reports. 2015;**5**:16014

[29] Lee D, Umer MA, Ryu HJ, Hong SH. The effect of HfC content on mechanical properties HfC–W composites. International Journal of Refractory Metals and Hard Materials. 2014;**44**:49-53

[30] Wang YK, Miao S, Xie ZM, Liu R, Zhang T, Fang QF, et al. Thermal stability and mechanical properties of HfC dispersion strengthened W alloys as plasma-facing components in fusion devices. Journal of Nuclear Materials. 2017;**492**:260-268

[31] Liu R, Xie ZM, Yao X, Zhang T, Wang XP, Hao T, et al. Recent progress on the R&D of W-ZrC alloys for plasma facing components in fusion devices. Nuclear Materials and Energy. 2018;**16**:191-206

[32] Veleva L, Oksiuta Z, Vogt U, et al. Sintering and characterization

of W–Y and W–Y$_2$O$_3$ materials. Fusion Engineering and Design. 2009;**84**(7-11):1920-1924

[33] Liu R, Zhou Y, Hao T, Zhang T, Wang XP, Liu CS, et al. Microwave synthesis and properties of fine-grained oxides dispersion strengthened tungsten. Journal of Nuclear Materials. 2012;**424**:171-175

[34] Zhao MY, Zhou ZG, Zhong M, Tan J, Lian YY, Liu X. Thermal shock behavior of fine grained W–Y$_2$O$_3$ materials fabricated via two different manufacturing technologies. Journal of Nuclear Materials. 2016;**470**:236

[35] Lian YY, Liu X, Feng F, Song JP, Yan BY, Wang YM, et al. Mechanical properties and thermal shock performance of W-Y$_2$O$_3$ composite prepared by high-energy-rate forging. Physica Scripta. 2017;**T170**:014044

[36] Battabyal M, Schblin R, Spatig P, Baluc N. W–2wt.%Y$_2$O$_3$ composite: Microstructure and mechanical properties. Materials Science and Engineering A. 2012;**538**:53

[37] Veleva L, Schaeublin R, Battabyal M, Plociski T, Baluc N. Investigation of microstructure and mechanical properties of W–Y and W–Y$_2$O$_3$ materials fabricated by powder metallurgy method. International Journal of Refractory Metals and Hard Materials. 2015;**50**:210-216

[38] Xie ZM, Liu R, Miao S, Zhang T, Wang XP, Fang QF, et al. Effect of high temperature swaging and annealing on the mechanical properties and thermal conductivity of W–Y$_2$O$_3$. Journal of Nuclear Materials. 2015;**464**:193-199

[39] Pintsuk G, Kurishita H, Linke J, Arakawa H, Matsuo S, Sakamoto T, et al. Thermal shock response of fine-and ultra-fine-grained tungsten-based materials. Physica Scripta. 2011;**T145**:014060

[40] Kurishita H, Kobayashi S, Nakai K, Ogawa T, Hasegawa A, Abe K, et al. Development of ultra-fine grained W–(0.25-0.8) wt% TiC and its superior resistance to neutron and 3 MeV He-ion irradiations. Journal of Nuclear Materials. 2008;**377**:34-40

[41] Li PF, Fan JL, Han Y, et al. Microstructure evolution and properties of tungsten reinforced by additions of ZrC. Rare Metal Materials and Engineering. 2018;**47**(6):1695-1699

[42] Xie ZM, Zhang T, Liu R, Fang QF, Miao S, Wang XP, et al. Grain growth behavior and mechanical properties of zirconium micro-alloyed and nano-size zirconium carbide dispersion strengthened tungsten alloys. International Journal of Refractory Metals and Hard Materials. 2015;**51**:180-187

[43] Liu R, Xie ZM, Yao X, Zhang T, Wang XP, Hao T, et al. Effects of swaging and annealing on the microstructure and mechanical properties of ZrC dispersion-strengthened tungsten. International Journal of Refractory Metals & Hard Materials. 2018;**76**:33-40

[44] Krsjak V, Wei SH, Antusch S, Dai Y. Mechanical properties of tungsten in the transition temperature range. Journal of Nuclear Materials. 2014;**450**:81-87

[45] Zhao M, Zhou Z, Zhong M, Tan J. Effect of hot rolling on the microstructure and fracture behavior of a bulk fine-grained W–Y$_2$O$_3$ alloy. Materials Science and Engineering: A. 2015;**646**:19-24

[46] Ishijima Y, Kannari S, Kurishita H, Hasegawa M, Hiraoka Y, Takida T, et al. Processing of fine-grained W materials without detrimental phases and their mechanical properties at 200-432 K. Materials Science and Engineering: A. 2008;**473**:7-15

[47] Guo HY, Xia M, Chan LC, Wang K, Zhang X-X, Yan Q-Z, et al. Nanostructured laminar tungsten alloy with improved ductility by surface mechanical attrition treatment. Scientific Reports. 2017;**7**:1351

[48] Miao S, Xie ZM, Zhang T, Wang XP, Fang QF, Liu CS, et al. Mechanical properties and thermal stability of rolled W-0.5 wt% TiC alloys. Materials Science and Engineering: A. 2016;**671**:87-95

[49] Miao S, Xie ZM, Yang XD, Liu R, Gao R, Zhang T, et al. International Journal of Refractory Metals and Hard Materials. 2016;**56**:8-17

[50] Fukuda M, Nogami S, Hasegawa A, et al. Tensile properties of K-doped W–3% Re. Fusion Engineering and Design. 2014;**89**(7-8):1033-1036

[51] Yin C, Bakaeva A, Terentyev D, Petrov R, Pardoen T, Antush S, et al. Tensile properties of baseline and advanced tungsten grades for fusion applications. International Journal of Refractory Metals and Hard Materials. 2018;**75**:153

[52] Wirtz M, Linke J, Loewenhoff T, Pintsuk G, Uytdenhouwen I. Transient heat load challenges for plasma-facing materials during long-term operation. Nuclear Materials and Energy. 2017;**12**:148-155

[53] Lian YY, Liu X, Cheng ZK, Wang J, Song JP, Yu Y, et al. Thermal shock performance of CVD tungsten coating at elevated temperatures. Journal of Nuclear Materials. 2014;**455**:371-375

[54] Uytdenhouwen I, Decreton M, Hirai T, Linke J, Pintsuk G, Van Oost G. Influence of recrystallization on thermal shock resistance of various tungsten grades. Journal of Nuclear Materials. 2007;**363**:1099-1103

[55] Zhang XX, Yan QZ. The thermal crack characteristics of rolled tungsten in different orientations. Journal of Nuclear Materials. 2014;**444**:428-434

[56] Huang B, Tang J, Chen LQ, Yang XL, Lian YY, Chen L, et al. Design of highly thermal-shock resistant tungsten alloys with nanoscaled intra-and inter-type K bubbles. Journal of Alloys and Compounds. 2019;**782**:149-159

[57] Zhang XX, Yan QZ, Lang ST, Xia M, Liu X, Ge CC. Thermal shock and fatigue resistance of tungsten materials under transient heat loading. Journal of Nuclear Materials. 2014;**455**:537-543

[58] Liu X, Lian YY, Greuner H, Boeswirth B, Jin YZ, Feng F, et al. Irradiation effects of hydrogen and helium plasma on different grade tungsten materials. Nuclear Materials and Energy. 2017;**12**:1314-1318

[59] Lu GH, Cheng L, Arshad K, Yuan Y, Wang J, Qin SY, et al. Development and optimization of STEP—a linear plasma device for plasma-material interaction studies. Fusion Science and Technology. 2017;**71**:177-186

[60] Ackland G. Controlling radiation damage. Science. 2010;**327**:1587-1588

[61] Zinkle SJ, Snead LL. Designing radiation resistance in materials for fusion energy. Annual Review of Materials Research. 2014;**44**:241-267

[62] Bai XM, Voter AF, Hoagland RG, Nastasi M, Uberuaga BP. Efficient annealing of radiation damage near grain boundaries via interstitial emission. Science. 2010;**327**:1631-1634

[63] Iwaoka H, Arita M, Horita Z. Hydrogen diffusion in ultrafine-grained palladium: Roles of dislocations and grain boundaries. Acta Materialia. 2016;**107**:168-177

[64] Du J, Höschen T, You JH. Feasibility study of a tungsten wire-reinforced tungsten matrix composite with ZrOx

interfacial coatings. Composites Science and Technology. 2010;**70**:1482-1489

[65] Du J, You JH, Höschen T. Thermal stability of the engineered interfaces in Wf/W composites. Journal of Materials Science. 2012;**47**:4706-4715

[66] Riesch J, Buffière J-Y, You JH, et al. In situ synchrotron tomography estimation of toughening effect by semi-ductile fibre reinforcement in a tungsten-fibre-reinforced tungsten composite system. Acta Materialia. 2013;**61**:7060-7071

[67] Riesch J, Höschen T, You JH. Enhanced toughness and stable crack propagation in a novel tungsten fibre-reinforced tungsten composite produced by chemical vapour infiltration. Physica Scripta. 2014;**T159**:014031

[68] Coenen JW, Antusch S, Aumann M, et al. Materials for DEMO and reactor applications—boundary conditions and new concepts. Physica Scripta. 2016;**T167**:014002

[69] Mao Y, Coenen JW, Riesch J, Sistla S, Almanstötter J, Jasper B, et al. Influence of the interface strength on the mechanical properties of discontinuous tungsten fiber-reinforced tungsten composites produced by field assisted sintering technology. Composites Part A Applied Science and Manufacturing. 2018;**107**:342-353

[70] Jiang Y, Zhang LH, Fang QF, Zhang T, Wang XP, Hao T, et al. Toughness enhancement of tungsten reinforced with short tungsten fibres. Materials Science and Engineering A. 2017;**690**:208-213

[71] Du J, Hochen T, Rasinski M, You J-H. Shear debonding behavior of a carbon-coated interface in a tungsten fiber-reinforced tungsten matrix composite. Journal of Nuclear Materials. 2011;**417**:472-476

[72] Riesch J, Han Y, Almanstötter J, Coenen JW, Höschen T, Jasper B, et al. Development of tungsten fibre-reinforced tungsten composites towards their use in DEMO—potassium doped tungsten wire. Physica Scripta. 2016;**T167**:014006

[73] Riesch J, Buffiere J-Y, Höschena T, Scheelc M, Linsmeiere C, You J-H. Crack bridging in as-fabricated and embrittled tungsten single fibre-reinforced tungsten composites shown by a novel in-situ high energy synchrotron tomography bending test. Nuclear Materials and Energy. 2018;**15**:1-12

[74] Avello de Lama M, Balden M, Greuner H, Höschen T, Matejicek J, You JH. Microstructural stability of spark-plasma-sintered Wf/W composite with zirconia interface coating under high-heat-flux hydrogen beam irradiation. Nuclear Materials and Energy. 2017;**13**:74-80

[75] Riesch J, Aumann M, Coenen JW, Gietl H, Holzner G, Höschen T, et al. Chemically deposited tungsten fibre-reinforced tungsten–the way to a mock-up for divertor applications. Nuclear Materials and Energy. 2016;**9**:75-83

[76] Linsmeier C, Rieth M, Aktaa J, et al. Development of advanced high heat flux and plasma-facing materials. Nuclear Fusion. 2016;**57**:092007